Strong electronic winds blowing under liquid flows on carbon surfaces

Alice Marcotte,[1,*] Mathieu Lizee,[1,*] Baptiste Coquinot,[1,2] Nikita Kavokine,[2] Karen Sobnath,[3] Clément Barraud,[3] Ankit Bhardwaj,[4,5] Boya Radha,[4,5] Antoine Niguès,[1] Lydéric Bocquet,[1] and Alessandro Siria[1]

[1] *Laboratoire de Physique de l'École Normale Supérieure, ENS, Université PSL, CNRS, 3 Sorbonne Université, Université Paris Cité, 75005 Paris, France*

[2] *Center for Computational Quantum Physics, Flatiron Institute, New York, USA*

[3] *Université Paris Cité, Laboratoire Matériaux et Phénomènes Quantiques, CNRS, F-75013 Paris, France*

[4] *National Graphene Institute, The University of Manchester, UK*

[5] *Department of Physics and Astronomy, The University of Manchester, UK*

Solid-liquid interfaces display a wealth of emerging phenomena at nanometre scales, which are at the root of their technological applications. While the interfacial structure and chemistry have been intensively explored, the potential coupling between liquid flows and the solid's electronic degrees of freedom has been broadly overlooked up till now. Despite several reports of electronic currents induced by liquids flowing in various carbon nanostructures, the mechanisms at stake remain controversial. Here, we unveil the molecular mechanisms of interfacial liquid-electron coupling by investigating flow-induced current generation at the nanoscale. We use a tuning fork Atomic Force Microscope (AFM) to deposit and displace a micrometric liquid droplet on a multilayer graphene sample, and observe an electronic current induced by the droplet displacement. The measured current is several orders of magnitude larger than previously reported for water on carbon, and further boosted by the presence of surface wrinkles on the carbon surface. Our results point to a peculiar momentum transfer mechanism between the fluid molecules and graphene charge carriers, mediated mainly by the solid's phonon excitations. These findings open new avenues for active control of nanoscale liquid flows through the solid walls' electronic degrees of freedom.

I. INTRODUCTION

The transport of liquids near carbon surfaces has unveiled a wide range of unexpected properties, ranging from very fast permeation to non-linear ion transport and sieving [1, 2], as well as promising applications in energy harvesting [3]. These results highlight the peculiar nature of the liquid-solid interaction. In a classical framework – such as the widely used force-field molecular dynamics simulations – a solid acts on fluid molecules as a static periodic potential, and the interfacial fluid dynamics are understood in terms of the atomic-scale surface roughness. Yet, a number of recent observations have challenged this conventional description by revealing couplings between liquid flows and the solid's electronic degrees of freedom. Prominent examples include liquid-flow-induced electronic currents [4–13], the modification of wetting by electronic screening [14, 15], or anomalies in the water-carbon friction [16]. This points to the need of understanding the molecular mechanisms at stake: in particular, several observations of flow-induced electronic currents [7] still lack a satisfactory rationalization.

In this article, we report the generation of an electric current in a few-layer graphene sample by the displacement of a liquid droplet. As opposed to previous reports, our experiment has sub-micrometer dimensions: such dimensions are incompatible with known current generation mechanisms, such as the charging/discharging of a pseudo-capacitance [12, 13]. With the help of a full theoretical investigation carried out in parallel with this work [17], we determine that the current generation is mainly due to droplet displacement exciting a phonon wind within the graphene sample, its magnitude being tuned by a subtle interplay between electron-phonon and electron-liquid Coulomb interactions.

The paper is organized as follows. In Section II we describe our experimental setup and the procedure for a typical experiment. Section III summarizes our quantitative results for the flow-induced electronic current across a wide range of samples and conditions. In Section IV, we outline our theoretical model, and Section V establishes our conclusions.

II. EXPERIMENTAL PROCEDURE

We deposited a thin graphite flake (1 to 70 nm in thickness) onto a Si/SiO_2 substrate; two gold electrodes, separated by a distance

* These authors contributed equally to this work

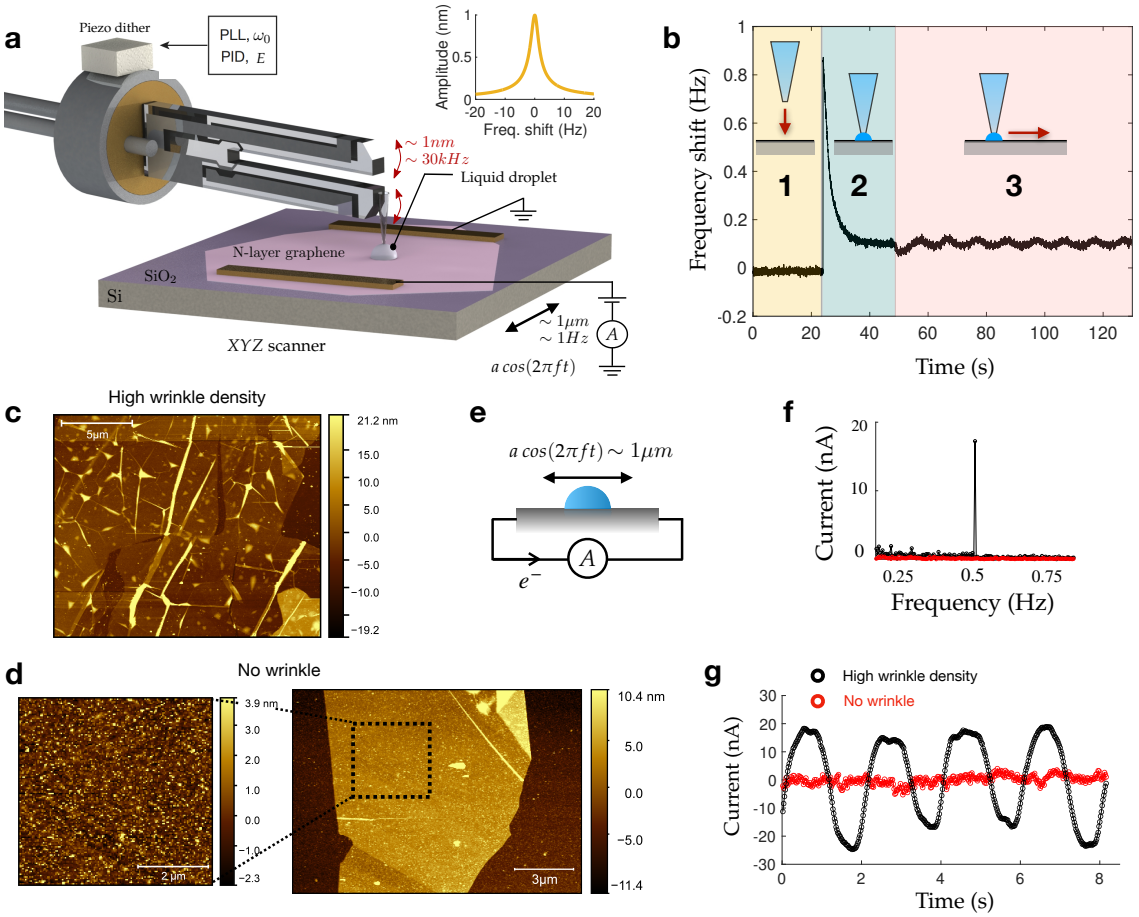

Figure 1: **Experimental set-up. a,** Schematic of the experiment. A quartz capillary of tip diameter of 500 nm is filled with liquid and glued on the lower prong of a millimetric quartz tuning fork. Once the tip is in contact with the graphite substrate, a liquid droplet is formed at its extremity. The scanner allows for droplet relative motion on the graphite flake in the XY-plane, while current is measured between both gold electrodes. An additional electric potential drop ΔV can be imposed between the electrodes. *Inset*: The resonance curve of the tuning fork whose frequency shift is used to deposit the droplet and maintain a gentle mechanical contact. **b,** Frequency shift response of the AFM during a typical experiment, indicating the stiffness of the pipette-sample contact. First, the pipette is brought into contact with the sample (1). After the contact, a slow relaxation (2) indicates the formation of the droplet. Finally, the sample is put into horizontal motion with respect to the droplet while a PID controller keeps a constant frequency shift (3). **c,** AFM image of a multilayer graphene sample (3.6 nm thick) exhibiting a high density of wrinkles. **d,** AFM image of a flat multilayer graphene sample (1.5 nm-thick). **e,** Schematic of droplet motion. **f,** The current spectrum as a function of frequency. For the wrinkled sample (black curve), the spectrum displays a peak at the droplet oscillation frequency (0.5 Hz). **g,** Current (nA) as a function of time (s) resulting from droplet oscillations of 2 μm amplitude and 0.5 Hz frequency, on the wrinkled sample displayed on **c** (black dots) and on the flat multilayer graphene sample displayed on **d** (red dots). We stress that the DC component of the current, induced by the drain-source bias, is substracted on panels **f** and **g**.

of $\sim 10\mu$m (see Figure S1 **c,f**) and connected to a low noise current amplifier, allowed us to measure the electric current passing through the flake. The sample was placed in a tuning fork atomic force microscope (AFM), that was specifically designed for controlled liquid deposition, see Figure 1**a**. The liquid was introduced into a quartz capillary, which was then glued to the quartz tuning fork (see Figure S1 **a,b**). A piezo-dither induced a nanometric oscillation of the tuning fork at its resonant frequency ($f_0 \approx$ 32 kHz), a typical resonance curve is shown in

the inset of Figure 1**a**. By monitoring precisely the tuning fork oscillation's phase and amplitude as the pipette tip approach the sample, we achieved a fully controlled contact between the carbon surface and the pipette's aperture, leading to the formation of a liquid capillary bridge. The capillary bridge then evolved into a droplet, of radius fixed by the outer diameter of the tip (500 nm) [18, 19]. This novel experimental set-up allows to deposit very viscous liquid at nano and micro scale over a broad range of substrates [20]. We used a room temperature ionic liquid (BMIM-PF6) and a neutral and apolar silicon oil (Polyphenyl-methylsiloxane), both very viscous with a viscosity of 0.3 Pa·s and 0.1 Pa·s, respectively, and with very small vapor pressures, allowing us to safely neglect evaporation. The continuous monitoring of the contact with both the in-situ optical microscope and the AFM frequency shift signal allows us to ensure that the droplet remained hooked to the tip, sliding over the carbon surface. Moreover, motion does preserve the roughly spherical shape of the droplet (see Figure S1**c**) and the amplitude of the tuning fork's vertical oscillation (1 nm) is several orders of magnitude smaller than the horizontal droplet's motion ($1\mu m$).

In a typical experiment, the droplet is put into oscillatory motion, horizontally on the carbon surface by a piezo-scanner with an amplitude of a few microns at a frequency of the order of 1 Hz. Driven by the pipette, the droplet is thus oscillating along a line between the two electrodes, of a few micrometer in length. An electric current through the carbon surface is then measured at the droplet oscillation frequency (Figure 1**e**). As shown on Figure 1**a**, our set-up enables to further impose a constant potential drop ΔV (typically between -50 mV and 50 mV) between the drain at potential ΔV and the grounded source. We report electric currents in the tens of nano-Ampere range induced by a droplet moving at a few micrometers per second in samples whose resistance ranges from 300Ω to $2k\Omega$. To allow for a comparison with other current generation experiments, we define the current density as the AC-current amplitude divided by the diameter of the droplet (of order 1μm) : $j = I/(2R_{\text{drop}})$ typically in the tens of nA/μm range.

Several benchmark measurements allowed us to ensure that the current generation is due to the specific interaction of the liquid droplet with the few-layer graphene. We checked that no alternating current is recorded when the deposited droplet oscillates over the SiO_2 substrate between the electrodes, outside the multilayer graphene substrate. We further controlled that no current is generated when the pipette is not in contact with the graphite but slightly above or even when a tungsten tip is used instead of the liquid filled pipette, see Figure S1 **d,e**. We also checked that the tuning fork's oscillation amplitude does not affect the results. Altogether, we can safely conclude that the measured effect is due to the displacement of the liquid droplet on the carbon surface.

III. ELECTRO-FLUIDIC CONDUCTIVITY

A. Scaling behavior

On Figure 2**a**, we report results of several samples (with thickness varying between 1.7 and 8.2 nm), where an electro-fluidic current is measured. We observe that for a fixed oscillation frequency f and bias voltage ΔV, the amplitude of the AC generated current increases linearly with the droplet oscillation amplitude a, or equivalently, with the droplet peak velocity ($v = 2\pi f a$). Taking advantage of the demonstrated linear dependency of the current density with respect to the droplet peak velocity, we define the electro-fluidic conductivity of our samples as

$$\sigma_{\text{ef}} = \frac{j}{v},$$

quantifying the cross-coupling between electronic current j and liquid flow v. Among the five samples presented here, we show an electro-fluidic conductivity ranging from 2.8 to 21.6 nA.s/μm^2 for a micrometric ionic liquid droplet. We stress that silicon oil yields an electro-fluidic conductivity of the same order of magnitude $\sigma_{\text{ef}} \sim 2$nA.s/$\mu$m^2(*cf*: Figure S1**g**).

To gain insight into the mechanism driving this electro-fluidic current and having in mind the strong dependence of the graphene electronic density on the local potential [21], we tune the bias voltage ΔV between the electrodes and measure its influence on the electro-fluidic current. We observe that the amplitude of the alternating current scales linearly with ΔV, as highlighted in Figure 2 **b, c**. We observe a small or negligible current at zero potential drop and we note that the current is phase-shifted by π between positive and negative values of the bias voltage (this is represented by the sign change in the amplitude).

Finally, the slope $\sigma_{\text{ef}}/\Delta V$ is in the range of 0.05 to 0.2 nA.s/μm^2/mV, see Figure 2**c**, with a slight variation across samples.

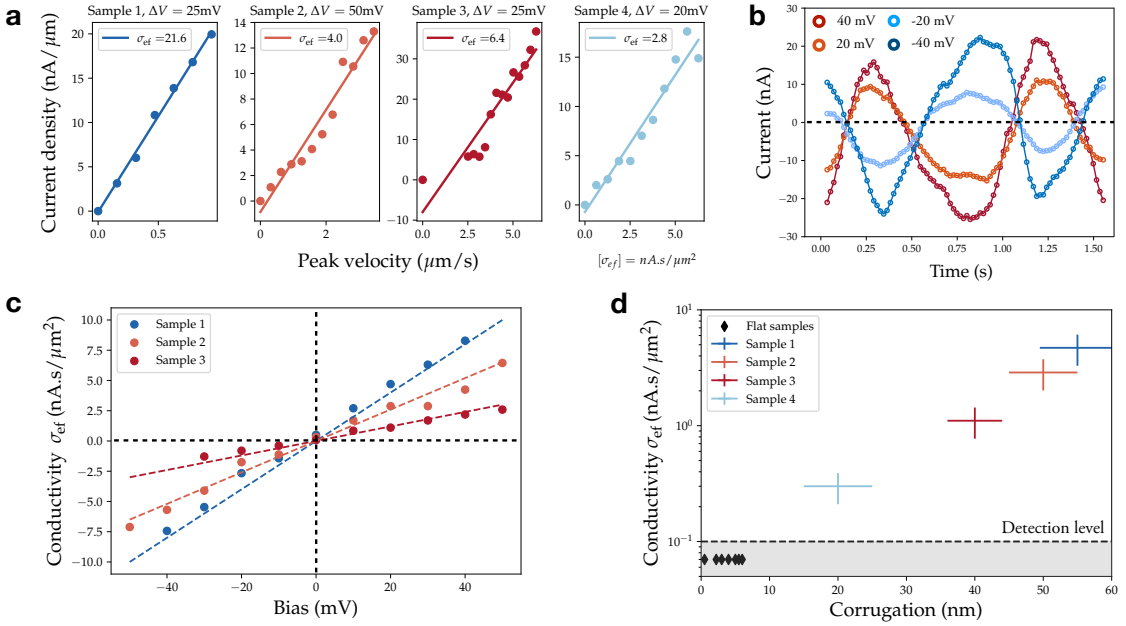

Figure 2: **Generation of a droplet motion-induced electronic current. a,** Current density (nA/μm) as a function of fluid velocity $v = 2\pi fa$ for 4 different samples. Each curve is measured at a bias ΔV indicated in the corresponding plot. The multi-layer graphene subtrates have thickness 3.3, 1.7, 3.6 and 8.2 nm, respectively and their corresponding surface roughness measured using AFM are [55,50,40,20] nm respectively. **b,** Time-dependent current under droplet oscillation for various voltage bias ΔV. **c,** Effect of the voltage bias ΔV on the electro-fluidic conductivity $\sigma_{\text{ef}} = j/v$, showing a linear dependency. The dotted lines are guides to the eye. **d**, Electro-fluidic conductivity σ_{ef} (at $\Delta V = 20$ mV) versus the substrate corrugation, measured using AFM images. The black diamonds correspond to current measurements below the detection level.

B. Wrinkles as current amplifiers

An unexpected feature of the experimental results is the sharp distinction among carbon samples regarding the amplitude of the the electro-fluidic conductivity. Across all samples, with thicknesses ranging from 1 nm up to 70 nm, we observe that the thinner ones tends to exhibit the largest electro-fluidic conductivity, see Figure S2**a**. However, investigating the surface topography of the carbon samples using AFM imaging, such as on Figure 1 **c-d**, we reveal that the correlation is rather between the amplitude of the electro-fluidic conductivity and the existence of surface corrugation in the forms of folds and wrinkles. Notably, thinner samples exhibit a large number of folds and wrinkles whereas thicker samples present a flat surface without folds or defects (see Figure S2 **c,d**). This difference is due to the fabrication process involving the transfer of the exfoliated graphene flake onto the oxidized silicon wafer (see Appendix A) : the thinner flakes are softer and more flexible than the thicker ones, and more likely to exhibit wrinkles [33, 34], see Figure S2 **c,d**. In order to disentangle the role of wrinkles from that of sample thickness, we implemented an alternative fabrication method in which all transfer steps are avoided and few-layer graphene flakes were directly exfoliated on the Si/SiO_2 wafer. This allowed us to obtain sub-10 nm, un-transferred and *smooth* graphene samples with a uniform wrinkle-free surface (see Figure 1 **c, d**) to compare with the *transferred* and *crumpled* flakes of similar thickness showing a much larger surface corrugation (see Appendix D and Figure S2 **g-j** for a Raman analysis of wrinkles). As shown on Figure 2**d** and Figure S2 **a**, droplet motion on smooth samples results in no detectable current. Conversely, crumpled flakes of the same thickness have a high wrinkle density and show the strongest electro-fluidic conductivity, in the nA.s/μm^2 range. Our results reveal that wrinkles are instrumental to the current generation mechanism, while there is no evidence of an effect of graphene thickness.

Further evidence of the crucial role of wrin-

kles is provided by the dependence of the generated current on the droplet oscillation direction, see Figure S2 **e,f**. As expected, the current amplitude is 180° periodic with respect to the angle between the droplet trajectory and the electrodes. However, the maximal amplitude is not necessarily reached when the droplet oscillation is perpendicular to the electrodes, and the direction yielding the maximum current strongly depends on the position on the sample's surface. We argue that this spatial and directional variability is related to the random distribution in height, position and direction of the wrinkles on the carbon surface. This further highlights the role of wrinkles as current amplifiers. Let us note for completeness that the data displayed on Figure 2 are obtained along the direction with maximal amplitude.

IV. PHONON DRAG MECHANISM

Summarizing our experimental results, we have shown that the motion of a micrometric droplet on a crumpled, few-layer graphene surface generates a strong electro-fluidic current in the flake, which is proportional to the velocity of the droplet, as well as to the bias voltage applied between the electrodes. A remarkable feature is the strong dependence of the magnitude of the generated current on the surface corrugation of the flake. While our results echo previous reports of electric potential differences induced by water flow in carbon-based nanomaterials [4–13, 25, 32], the nanoscale dimensions of our experiment put us in position to disentangle various effects at the root of electronic current generation, and obtain insights into the molecular mechanism underlying the phenomenon. Previously, several mechanisms have been invoked to rationalize electro-fluidic currents, including streaming potential effects [5], adsorbed/desorbed ion hopping [8, 25], Coulomb drag [4, 7] or charging/discharging of a pseudo-capacitance [12, 13]. These mechanisms rely on Coulomb interactions between the polar liquid – that carries molecular partial charges – and the carbon surface as the main pathway for momentum transfer from the liquid to the electrons. However, the strong impact of surface corrugation suggests that, in the present case, current generation requires 'mechanical' transfer of momentum from the fluid to the charge carriers. In order to confirm this hypothesis, we repeated the experiment, with an apolar silicone oil instead of the ionic liquid (and a wrinkled few-layer graphene as a substrate). We observed qualitatively and quantitatively similar current generation (Figure S1 **g**): liquid-solid Coulomb interactions are therefore not instrumental to the underlying mechanism.

This conclusion led us to consider a phonon-drag-based mechanism, as first proposed theoretically in ref. [32]. Phonon drag relies on hydrodynamic (viscous) friction at the solid-liquid interface, which transfers momentum to the solid's phonons, thereby exciting a 'phonon wind'. Through the electron-phonon interaction, the phonon wind 'blows' on the Fermi sea, so that electrons near the Fermi surface are dragged along the direction of the liquid flow, hence producing an electric current (see Figure 3**a**). A complete quantum description of phonon drag, within the non-equilibrium Keldysh framework, is developed in the accompanying theoretical paper [17]. Here, we give only a semi quantitative description that allows us to capture the main physical ingredients.

First, assuming a Couette flow within the liquid droplet, the hydrodynamic friction force is $\mathbf{F}_0 \sim \eta \mathcal{A}_{\rm drop} \mathbf{v}_{\rm drop}/h_{\rm drop}$, $v_{\rm drop}$ is the drop velocity, η its viscosity, $\mathcal{A}_{\rm drop}$ its surface and $h_{\rm drop}$ its height (here typically, $\eta = 0.3\,\mathrm{Pa}\cdot\mathrm{s}$ and $h_{\rm drop} \approx 1\,\mu$m). In line with observations, wrinkles are expected to enhance this hydrodynamic friction force. In a simple picture, wrinkles are modelled as protusions on which the flowing liquid exerts a Stokes force that scales (per wrinkle) as $\mathbf{F}_{\rm W} \propto \eta h_{\rm W} \mathbf{v}_{\rm drop}$, where $h_{\rm W}$ is the typical height of the wrinkles ($h_{\rm W} \sim 10 - 30$ nm). One then obtains a total friction force $\mathbf{F}_{\rm W} \sim \mathbf{F}_0(1+W)$, where we introduced the dimensionless wrinkling number, $W = 3\pi n_{\rm W} h_{\rm W} h_{\rm drop}$ ($n_{\rm W}$ is the wrinkle density) to account for the increase in viscous friction due to surface corrugation. We emphasize that our approach relies on a momentum balance between the fluid and the solid. Hence the analysis does not depend crucially on the specific nature of the liquid flow. The Couette flow is merely a first approximation to the flow which is sufficient to obtain an estimate of the friction force.

A simplified sketch of our theoretical model is shown in Figure 3 **a-d**. The hydrodynamic friction force transfers momentum from the liquid (Figure 3**a**) to the solid's acoustic phonons, which have a dispersion relation $\epsilon_{\mathbf{q}} = \hbar q c$, c being the phonon (sound) velocity ($c \approx 2 \times 10^4$ m $\cdot$ s^{-1} [35, 37, 38]). The phonons relax mainly by transferring their momentum to the underlying substrate (Figure 3**d**) through Umklapp processes [35], on a typical timescale $\tau_{\rm um} \sim 10$ ps [36]. As sketched on Figure 3**b**, the constant influx of momen-

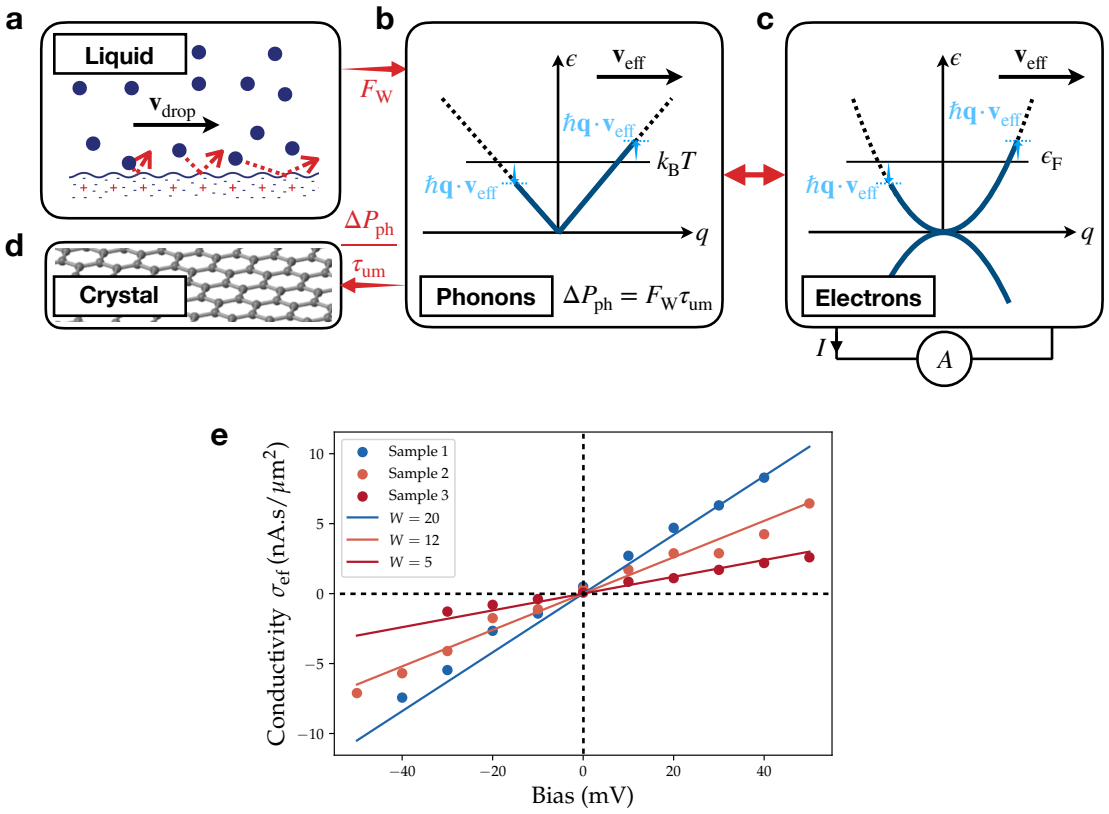

Figure 3: **Phonon drag mechanism.** The flowing liquid **a** exerts a friction force $F_{\rm W}$ on the graphite sample. This force is related to a momentum transfer to the phonons, that generates an asymmetry in the phonon distribution **b** which is biased in the direction of the liquid flow. Finally this asymmetry propagates to the electronic distribution **c** by electron-phonon interaction. This asymmetry in the electronic distribution translates into the generation of a net electric current, whose sign depends on the nature of charge carriers at the Fermi level (electrons or holes). We stress that this is an out of equilibrium phenomenon in which most of the momentum is relaxed to the crystal **d** by the Umklapp process with a rate $1/\tau_{\rm um}$. Finally, on **e**, we compare the theoretical derivation of the electro-fluidic conductivity $\sigma_{\rm ef}$ versus the bias voltage ΔV. We stress that the experimental data is the same as in Figure 2**c** and that the solid lines are plotted using Eq. (5) assuming the bulk graphite effective mass $m = 0.1m_{\rm e}$ and W the wrinkling number as the only fitting parameter chosen between 5 and 20. This wrinkling number characterizes the enhancement of Stokes friction due to wrinkles on the graphene surface.

tum can be modeled by a 'Doppler shift' in the phonon distribution, according to $\epsilon_{\mathbf{q}} \mapsto \epsilon_{\mathbf{q}} - \hbar\mathbf{q}\cdot\mathbf{v}_{\rm ph}$. Here $\mathbf{v}_{\rm ph}$ is the velocity of the phonon wind: it is determined by balancing the momentum fluxes in and out of the phonon system, according to $\tau_{\rm um}\mathbf{F}_{\rm W}/\mathcal{A}_{\rm drop} = \Delta\mathbf{P}_{\rm ph}/\mathcal{A}_{\rm drop} = \int \frac{{\rm d}\mathbf{q}}{2\pi}\hbar\mathbf{q}\, n_{\rm B}(\hbar qc - \hbar\mathbf{q}\cdot\mathbf{v}_{\rm ph})$, with $n_{\rm B}$ the Bose-Einstein distribution and $\mathbf{q}$ is the phonon wavevector, that we assume two-dimensional. This yields

$$\mathbf{v}_{\rm ph} \simeq \frac{2\pi}{3\zeta(3)}\frac{\hbar^2c^4}{(k_BT)^3}\times(1+W)\eta\frac{\mathbf{v}_{\rm drop}}{h_{\rm drop}}\times\tau_{\rm um} \quad (1)$$

Then, $v_{\rm ph} \approx 9\cdot 10^4 \times (1+W)\times v_{\rm drop}$.

As the electrons scatter on the phonons, they acquire an average 'wind' velocity $\mathbf{v}_{\rm e}$. If the direct liquid-electron Coulomb interaction is negligible, as considered in the simplified model of Figure 3 **a-d**, the electronic wind velocity aligns to the phonon wind velocity ($\mathbf{v}_{\rm e} \approx \mathbf{v}_{\rm ph}$), regardless of the form of the electron-phonon interaction [17]: this is a good approximation in the case of an apolar liquid. If the liquid is polar, our full theoretical analysis [17] shows that the electronic wind velocity is in fact given by a linear combination of the phonon wind and interfacial flow velocities:

$$\mathbf{v}_{\rm e} = \frac{\tau}{\tau^{\rm e/ph}}\mathbf{v}_{\rm ph} + \frac{\tau}{\tau^{\rm e/h}}\mathbf{v}_{\ell}. \quad (2)$$

Here $\tau^{\rm e/ph}$ and $\tau^{\rm e/h}$ are the typical electron-

phonon and electron-liquid scattering times, respectively, and $\tau^{-1} = (\tau^{\mathrm{e/ph}})^{-1} + (\tau^{\mathrm{e/h}})^{-1}$ is the total electron scattering rate near the Fermi surface. According to eq. (1), $v_\ell < v_{\mathrm{drop}} \ll v_{\mathrm{ph}}$, but, at the same time, the electron-phonon and electron-liquid scattering times have a similar order of magnitude [17]. Therefore, the electronic wind induced by a polar liquid is given by $\mathbf{v}_e \approx \mathbf{v}_{\mathrm{ph}}/2$: the liquid-electron Coulomb interactions actually contribute to reducing the flow-induced current. Accounting for the electronic wind amounts, again, to a Doppler shift of the electron dispersion in momentum space: $\epsilon_{\mathbf{q}} \mapsto \epsilon_{\mathbf{q}} - \hbar\mathbf{q}\cdot\mathbf{v}_{\mathrm{e}}$.

Assuming for concreteness that the liquid flows to the right, this roughly means that in an energy window of width $\hbar k_{\mathrm{F}} v_{\mathrm{eff}}$ around the Fermi level (k_{F} is the Fermi wavevector), the electrons move to the right at the Fermi velocity v_{F}. The corresponding current density reads

$$\mathbf{j} \approx e v_{\mathrm{F}} \times N(\epsilon_{\mathrm{F}}) \times [\hbar k_{\mathrm{F}} \mathbf{v}_{\mathrm{e}}], \tag{3}$$

where $N(\epsilon_{\mathrm{F}})$ is the density of states at the Fermi level ϵ_{F}. This simple expression is in fact consistent with the low-temperature limit of our full derivation [17], and provides enough quantitative accuracy for a comparison with experimental results. Equation (3) predicts a current density proportional to the droplet velocity, to the liquid viscosity and to the wrinkling number W, in excellent agreement with the experiment. Moreover, the current is independent (up to a factor of at most 2 that depends on the liquid polarity) of the chemical nature of the liquid, consistently with a similar amount of current being generated by ionic liquid and silicone oil droplets.

Although the graphene electronic bands have a linear dispersion, the electronic structure our multilayer samples of few-nanometer thickness (see Figure S2**a**) is expected to be better described by two touching parabolic band with effective mass $m \sim \pm 0.1 m_e$ (m_e being the free electron mass) [39–41]: $\epsilon_{\mathbf{q}} = \pm\hbar^2 q^2/2m$. The density of states is then independent of energy: $N(\epsilon) = N(\epsilon_{\mathrm{F}}) = m/\hbar^2$. Altogether, we obtain the electro-fluidic conductivity as

$$\sigma_{\mathrm{ef}} = e\frac{m}{\hbar^2}\epsilon_{\mathrm{F}} \times \frac{v_{\mathrm{e}}}{v_{\mathrm{drop}}}. \tag{4}$$

The prediction in Eq. (4) can now be compared quantitatively with experimental results. Experimentally, the bias voltage modifies the local potential at the droplet position, setting the Fermi level $\epsilon_{\mathrm{F}} \approx e\Delta V/2$, so that

$$\sigma_{\mathrm{ef}} \approx 0.1 \times m/m_{\mathrm{e}} \times (1+W) \times \Delta V \,[\mathrm{nA.s}/\mu\mathrm{m}^2] \tag{5}$$

with ΔV in mV. This estimate quantitatively reproduces the experimentally measured conductivity of a few nA.s/μm^2 as well as its linear scaling with the bias voltage. We note as well that the current is expected to change sign if the charge carriers are holes instead of electrons. This explains why the generated current flips sign along with ΔV: for positive bias, the charge carriers are electrons in the conduction band, whereas for negative bias, the charge carriers are holes in the valence band (a seamless transition is ensured by the fact that the bands are touching). In Figure 3**e**, we compare our theoretical prediction with the experimental results for σ_{ef} and observe indeed quantitative agreement, the only fitting parameter being the wrinkling number W, chosen between 5 and 20. Having developed the qualitative picture of phonon drag induced current and provided a quantitative comparison to experiments, we now discuss briefly the role of wrinkles as current amplifiers. In our drag-increasing-protrusion picture, wrinkles enhance the momentum transfer between the fluid and solid by actively increasing the interfacial friction force. In addition to this effect, it is known that wrinkles induce large strain gradients [43] (see Appendix D and figure S2g-j for Raman maps), locally enhancing the electron-phonon scattering and thus the momentum transfer from phononic to electronic distribution. While our interpretation provides a quantitativaley consistent explanation, one cannot rule out such enhanced scattering effects and they may indeed contribute to current enhancement pointing out the important role of local structure to phonon drag phenomenon.

Altogether, our theoretical description strongly supports the hypothesis that the experimentally observed current is due to the graphene charge carriers being dragged by a phonon wind induced by the liquid flow. In the accompanying theoretical paper [17], we further predict that such a mechanism leads to a *quantum feedback* phenomenon, where the electrons return part of the momentum acquired from the phonon wind back to the liquid: this is the reason why the electron wind velocity cannot align to phonon wind if the flowing liquid is polar (see eq. (2)). The quantum feedback leads to an apparent reduction of the hydrodynamic friction; measuring this 'negative friction' is beyond the scope the present experiments. At the relatively low electronic densities achieved in our samples, we would expect a friction reduction of at most a few percent [17]. Specific friction measurements in samples with higher electronic

density of states, where the effect is expected to be macroscopic, will be the subject of future work.

V. CONCLUSIONS

We report the generation of a very large electronic current density induced by the controlled motion of a liquid droplet at the surface of carbon nanomaterials. Our results suggest that the current generation is mediated by hydrodynamic momentum transfer from the flowing liquid to the phonons in the solid. Our specifically tailored system is particularly well-suited to evidence this phonon drag mechanism. Indeed, the combination of a local micrometric flow on strongly wrinkled graphene samples with the high viscosity of the neutral liquids allows the phonon drag to dominate current generation. The versatility of our setup enables us to tune the fluid velocity as well as the solid's electronic properties using the bias between the electrodes to fully characterize the phenomenon.

The experimental results were rationalized with a new dedicated theoretical model. The experimental evidence for the basic phonon drag mechanism is promising for the observations of further predictions of our theory, including the quantum feedback mechanism and 'negative friction'. Our findings pave the way for the active control of fluid transport at the nanoscale, by harnessing the interplay between molecular liquid flows and collective excitation within the solid. They further stimulate the development of small footprint flow sensing devices which could allow simultaneous measurement of interfacial velocity and viscosity. Finally, the coupling of electronic and microfluidic currents bears the promise of ubiquitous and environment-friendly energy production, as demonstrated recently in transpiration-driven electrokinetic power generators [42].

APPENDIX A : GRAPHENE-BASED DEVICE'S MICRO-FABRICATION

A. Transferred samples

The HOPG crystals are purchased from HQ Graphene. Each bulk crystal is mechanically exfoliated and flakes are first randomly deposited on separate 280 nm-thick Si/SiO2 substrates. Graphene flakes are then carefully selected for their thickness (ranging from 1 nm to 70 nm), homogeneity and size (> 15 μm). The graphene flakes are transferred thanks to the "hot pick-up" technique known to produce clean and contamination free surfaces [24, 27] in a 100 x 100 μm^2 area in the middle of a 2x2 mm^2 prepatterned substrate with Au electrodes. The devices are then fabricated by defining two parallel electrical contacts over the graphene flake by e-beam lithography using a double layered PMMA process: a 50 K lower layer of PMMA and a 950 K upper layer of PMMA both spin-coated at 4000 RPM. The spacing between the two contacts is set to at least 10 μm for the AFM experiment. The metallic contacts are subsequently deposited under high vacuum (a few 10-7 mBar) by e-beam evaporation. 5 nm of Ti covered by 45 nm of Au are deposited at very low evaporation rates (0.1 nm/s). The last fabrication step is a lift-off process in which the remaining resist is dissolved in an aceton bath for 20 min. The samples are finally rinsed into isopropanol for 2 min. This fabrication method involves a transfer of the graphite flake and thus yields a high density of wrinkles on thinner flakes as measured by AFM (*cf:* Figure S2**c**). Thicker flakes on the other hand do not show any tranfer-induced wrinkles (*cf:* Figure S2**d**). Before the experiment, we verify by AFM imaging that the samples are free of contamination.

B. Un-transferred samples

As discussed in the text, wrinkles have a strong influence on viscous flow driven current generation at the carbon surface. To assess the role of wrinkles in current generation, we used a transfer-free fabrication technique to prepare flat graphite samples. We evaporated gold electrodes on the SiO2 substrate where the graphite was exfoliated in the first place and thus obtained wrinkle-free samples (Figure S2**b**) which can be compared to high wrinkle-density (Figure S2**c**) samples of the same thickness obtained when transferring the flakes before evaporating the contacts.

APPENDIX B: DROPLET MOTION-INDUCED CURRENT GENERATION

a. Micro-pipette AFM preparation The capillary tip is obtained by locally heating and simultaneously pulling a 10 cm long quartz capillary of inner diameter 0.5 mm and outer diameter 1 mm (World Precision Instruments), with a Sutter Instruments P-2000 pipette puller. We obtain tips with an outer diameter of 500 nm

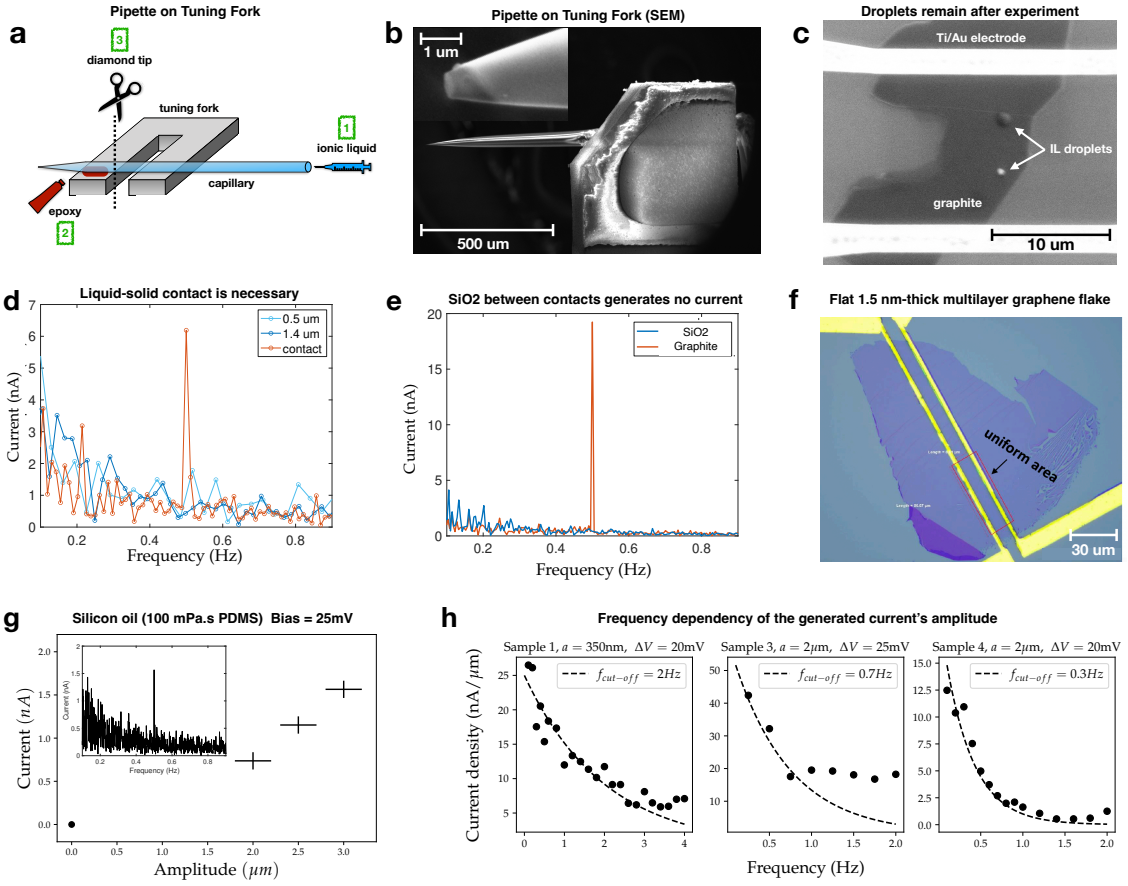

Figure S1: **Experimental techniques a** Steps for the preparation of the tuning fork and its probe: Firstly, the pipette is filled with liquid. Then, it is glued with epoxy on the side of one tuning fork prong. Finally, the cylindrical part of the capillary is cut free from its extremity and from the tuning fork with a diamond tip. **b** Scanning Electron Microscopy images of the lower prong of a millimetric tuning-fork, and of the extremity of the pipette glued on it (*inset*). The pipette's diameter is measured from such SEM images. **c** Post-experiment Scanning Electron Microscopy image of a graphite sample. Two roughly spherical ionic liquid droplets remain on the flake. **d** Current spectrum (nA) as a function of the frequency (Hz) while the capillary tip moves at 5 μm amplitude and 0.5 Hz frequency above the sample (0.5 μm on light blue curve and 1.4 μm on dark blue curve) and in contact with the graphite *via* the ionic liquid droplet (red curve). **e** Current spectrum (nA) as a function of the frequency (Hz) for a droplet motion on graphite (red curve) and on SiO_2 (blue curve). **f** Optical microscope image of a flat graphene flake with the gold electrodes clearly visible. This flake has not been transferred. **g** Generated current amplitude as a function of the silicon oil droplet oscillation amplitude, at 0.5 Hz and a bias voltage $\Delta V = 25mV$. The circles are the experimental data, while the dotted line is the best linear fit. We extract $\sigma_{\text{ef}} \sim 2nA.s/\mu m^2$. The inset is measured for a 3 μm oscillation amplitude. **h** Generated current density as a function of the oscillation frequency. We show the dependency measured on three different samples (corresponding to those described previously) namely samples 1, 3 and 4. The oscillation amplitude and bias are given above each plot. An exponential decay of decay frequency $f_{cut-off} \in \{2, 0.7, 0.3\}\, Hz$ is also shown for each sample.

(measured by SEM), that can be varied by tuning the pulling parameters. The pipette is then filled with ionic liquid (Bmim-PF6 of high purity from Merck) or with neutral silicon oil (Polyphenyl-methylsiloxane, 100 mPa.s, from Sigma Aldrich). Once the pipette is filled, its very extremity is glued with epoxy glue on the lateral side of a millimetric quartz tuning fork prong. With a diamond tip, the largest part of the capillary is then cut free from its extremity and from the tuning fork. These steps are summarized on Figure S1**a**. Finally, the tuning

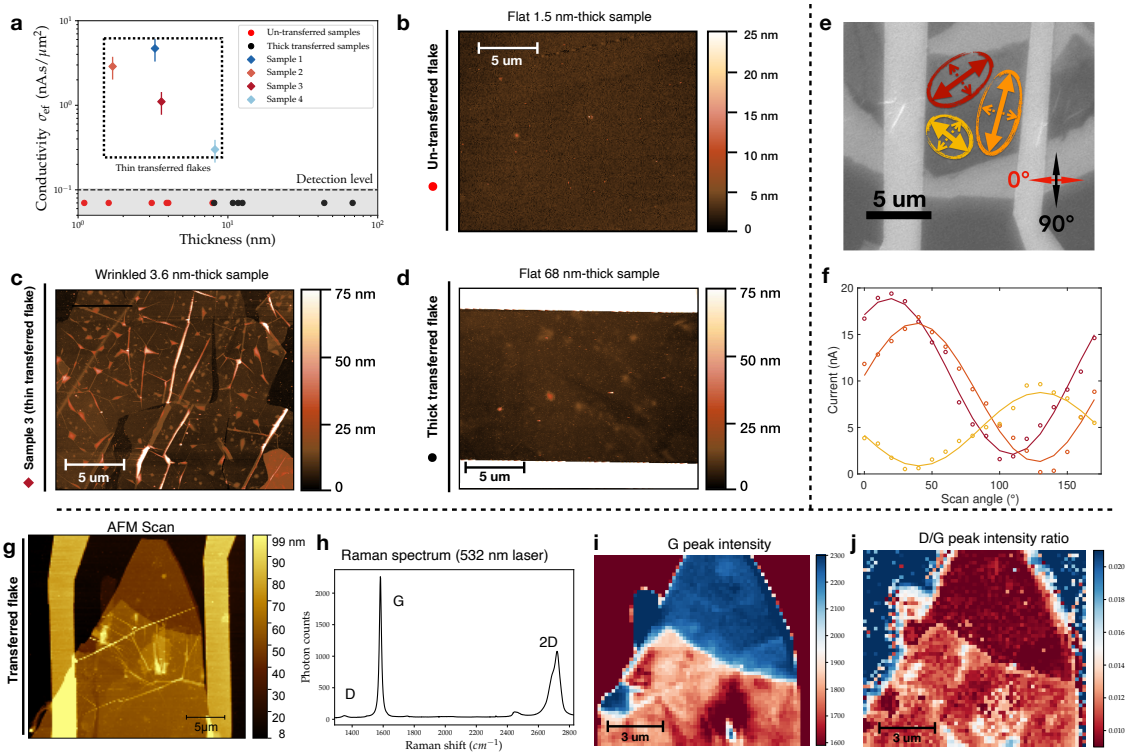

Figure S2: **Influence of wrinkles on graphene surface a** Log-log plot of the electro-fluidic conductivity given in $nA.s/\mu m^2$, as a function of the flake thickness. We clearly show that the fluctuations of electro-fluidic conductivity are dominated by corrugation and not flake thickness (*cf :* Figure 2**d**). **b** AFM image of a flat 1.5 nm-thick sample (un-transferred). **c** AFM image of a current generating wrinkled 3.6 nm-thick sample (transferred). **d** AFM image of a flat 68 nm-thick sample (transferred). On **e**, we show a scanning electron microscopy image of a graphite sample. with a cartoon of the angular dependency of the generated current. Current is generated by droplet motion of constant amplitude and frequency, along axis forming tilted with respect to the electrode axis by the 'scan angle'. We stress that **e** is a schematic and that our in-situ microscope does not allow such a fine positioning. Here, as detailed on **f**, we show that the angular dependency of the generated current also depends of the region of the sample that we are scanning. **f** Generated current (nA) as a function of the scan angle (°) of droplet motion (at 0.5 Hz frequency and 1 μm amplitude), around various central positions. As expected, the current is a 180°-periodic function of the angle. For each location, the experimental points are pictured by circles, while the solid line is the best sinusoidal fit. This spatial and angular heterogeneity along with the importance of wrinkles is a clear argument for a direct momentum transfer mechanism. On **g**, we show an AFM scan of a wrinkled flake with its electrodes on which we performed extensive Raman spectroscopy. On **h**, a typical Raman spectrum is shown. The Raman G-peak intensity is displayed on **i** and is stronger in the thicker regions. On **j**, the intensity ratio between the D and G peak is displayed. The low value (1%) of this ratio indicate a very low level of defects. Moreover, wrinkles, as opposed to flake edges do not display any local D-peak enhancement. This indicates that wrinkles are indeed folded graphene structures and neither pollution nor defects.

fork and its probe are examined under Scanning Electron Microscopy, to measure the outer diameter of the pipette extremity and to make sure the previous fabrication steps did not damage the tip, see Figure S1**b**.

Liquid droplet creation and control All our experiments are conducted under ambient conditions. We deposit a small amount of liquid and move it over the sample while keeping constant geometrical properties of the droplet as well as mechanical constraints. As a liquid micro-manipulation tool, we use the quartz-tuning fork as an autosensitive Atomic Force Microscope (AFM) mechanical oscillator. The tuning fork is excited *via* a piezo-dither at its resonance frequency f_0 in the normal mode

($f_0 \approx 32$ kHz), while the amplitude and phase shift of the tuning fork oscillations with regards to the excitation AC voltage are obtained from the piezoelectric current through the tuning fork electrodes. Our home-made AFM is used in frequency-modulation mode : a Phase Lock Loop (PLL) ensures that the tuning fork is systematically excited at its resonant frequency and a PID servo loop maintains a constant oscillation amplitude by tuning the excitation voltage. Interactions with the substrate are detected by the change in the resonance frequency and in the excitation voltage. As shown on Figure 1 **a,b**, we monitor the gentle approach *via* the PLL to detect contact with the substrate and the formation of the capillary bridge, and to ensure a constant contact stiffness (frequency-shift) during the droplet motion on the sample. We stress that the pipette allows us to entrain the liquid droplet and accordingly move the liquid. The liquid droplet is substantially larger than the area of the pipette facing the substrate, and the pipette does not confine the liquid *per se*. Experiments actually do not exhibit a dependence of the induced current on confinement, which may vary from experiment to experiment.

Current measurement The sample's motion is controlled by a XYZ-scanner. Once the droplet is formed on the graphite sample, the X and Y position of the scanner are modulated by a Lock-In at the chosen amplitude (between 100 nm and a few microns) and at the chosen frequency (between 100 mHz and a few Hertz) while the electric current flowing through the electrodes on the graphite sample is demodulated at the droplet oscillation frequency. The direction of the droplet oscillation can be chosen, this allows to vary the angle between the droplet's motion axis and the inter-electrodes axis. Prior to any measurement of the generated current dependency on the modulation amplitude, we search for the scan angle leading to an alternating current with maximal amplitude, for a given frequency and amplitude of oscillations, around a given central position. Then we measure around the same central position and along the optimal axis the dependency of the generated current on the bias voltage ΔV. We verify that the tuning fork amplitude and the frequency shift (pipette-sample contact stiffness) have no influence on the generated current.

Shape-preserving motion of the droplet To make sure the reported phenomena are not related to a modification of the surface (painting) by the repeated flow of liquid, we imaged the samples after the measurements under Scanning Electron Microscopy. As shown on Figure S1**c**, the remaining droplets display a roughly spherical shape, which confirms that scanning of the sample with the capillary tip does not result in the deposition of a liquid line, but instead, in the sliding of a hemispherical droplet over graphite.

Slippage Considering the existing literature and experiments reported by several group where the slip length on multilayer graphene/SiO2 to be in the range of few nanometers at most [45, 46], we do not expect any slip flow effect to be relevant in our experiment. Indeed the size of the drop of liquid governed by the shape of the end of the pipette and always in the micrometer range. Any slippage effect is expected to scale like the ratio between the slip length and the size of the drop: therefore only a correction in the order of 1% can be induced by slippage.

Definition of σ_{ef} We chose to normalize the susceptibility of our experiment by the droplet's diameter thus defining the electrofluidic conductivity as a current divided by a velocity times a diameter. Although one could expect a dependency on the droplet's surface, this is not what our theoretical analysis predicts and we opted for this option to ease the comparison with theory. Still, as the droplet is a half sphere $1\mu m$ diameter, the surface normalized conductivity can be easily recovered as $\sigma_{ef}/0.75\mu m$.

APPENDIX C : CONTROLS

To make sure that the measured current is indeed related to the viscous flow of liquid on graphite, we performed extensive controls which we detail here. Firstly, the cleanliness of the samples is checked with AFM and airborne contaminants are removed by annealing in Ar atmosphere. We have not seen any impact of this annealing, this suggests that airborne contamination is irrelevant in the current generation mechanism. We measure the current in various experimental configurations and show that the motion of a viscous droplet on top of the graphite flake is necessary to measure a non-zero current. Finally, we demonstrate the irrelevance of charge or polarity of the liquid in the measured current by showing that neutral silicon oil generates the same current as ionic liquid of similar viscosity.

Using a tungsten tip instead of a liquid filled pipette To ensure that the generated current is linked to the specific liquid-graphene interaction, we firstly check that moving a tungten tip (micrometric radius of curvature) on the surface

does not generate any current. This proves that liquid friction is required and rules out generation mechanisms linked to moving impurities below the multilayer graphene.

Pipette above the droplet We first checked that no current can be generated if the pipette is not in contact with the liquid droplet but is slightly above instead (see Figure S1**d**). In this configuration, a liquid droplet is deposited on graphite and the pipette is subsequently retracted and brought a few μm above the liquid. Thus, during the oscillation, no motion is induced between the droplet and the sample. As shown on Figure S1**d**, we do not measure any motion induced current in this situation (even if the pipette is only 500 nm above the flake). This rules out any coupling between high voltage signal driving the scanner and the generated current as well as a coupling between trapped charges in the quartz and electronic currents. To further rule out the latter effect, we highlight that the screening length in the ionic liquid we used is much smaller (nm, [44]) than the droplet's height (μm).

On SiO_2 We also checked that no current can be generated if the droplet moves over the SiO_2 surface between the electrodes, see Figure S1**e**. These controls show unambiguously that current generation requires the droplet to slide on the graphite surface.

With a neutral and apolar silicon oil droplet Finally, we performed an additional control to confirm a mechanism relying on momentum transfer-mediated current generation by using neutral and apolar silicon oil (Polyphenylmethylsiloxane) instead of ionic liquid. This polymer is chosen to have viscosity close to the one of the ionic liquid (0.1 Pa.s instead of 0.3 Pa.s for the ionic liquid). As evidenced by Figure S1**g** the current generation is also possible in this configuration with induced currents of the same order of magnitude than with ionic liquid. Converting to electro-fluidic conductivity yields $\sigma_{\text{ef}} \sim 2nA.s/\mu m^2$ for 0.5Hz, 1 μm oscillation amplitude and 25 mV bias voltage which compares well to measurements on ionic liquids. This confirms that viscosity and thus a direct momentum transfer to the solid dominates any electrostatic contribution in the current we observe.

Frequency dependency of generated current The generated current displays a puzzling dependency on the oscillation frequency. At fixed oscillation amplitude, the current amplitude decreases with frequency making the droplet-graphite system a low-pass filter with a cut-off frequency in the order of 1 Hz (*cf:* Figure S1 **h**). This behavior cannot come from the solid state where electrons and phonons relax much faster. Thus, we attribute this behavior to a thin wetting film spread on the droplet trajectory, which would reduce the effective friction (and therefore the generated current) and could have such slow dynamics. Still, on a second timescale, dewetting takes place and the hemispherical droplet shown in Figure S1**c** reforms. In this scenario, increasing the frequency is not equivalent to increasing the oscillation amplitude. This dynamic behavior is very difficult to probe and rationalize as dewetting timescales strongly depend on surface cleanliness and possible contaminations on the graphene surface. We leave this intriguing dependency as a basis for future investigations and as shown on Figure S1 **h**, report a cut-off frequency in the 1 Hz range.

APPENDIX D : TRANSFER-INDUCED WRINKLES ON THINNEST FLAKES CONTROL THE GENERATED CURRENT

As discussed previously, our sample fabrication techniques allow us to produce graphite flakes of desired thickness with either a high wrinkle density (transferred flakes) or a very flat surface showing negligible roughness (untransferred flakes). We were therefore able to study the dependency of generated current on both thickness and wrinkle density independently. On Figure S2**a**, we illustrate the thickness-dependency of the current induced by droplet oscillations of 1 μm.s^{-1} for both transferred (diamonds) and un-transferred (circles) graphite flakes. Our experiments reveal that for transferred samples, the thinner the graphite flake, the more efficient the current generation. Primarily, we observe a transition for the current generation around 10 nm in thickness: for flakes thicker than 10 nm, no current generation is possible, while current can be induced at the surface of flakes thinner than 10 nm. On the other hand, we report no generated current for flat un-transferred samples down to single nanometer thickness. Like we detailed above and shown on Figures 2**d** and S2**a**, the thickness dependency is only apparent and the generated current is in fact determined by the sample's corrugation. As thinner flakes show a higher corrugation after the transfer, we observe an apparent dependency on flake thickness for the transferred flakes. Another experimental evidence of the predominant role played by the wrinkles resides in the strong spatial anisotropy of the generated current (*cf:* Figure S2 **e,f**). On

Figure S2**e**, we show a scanning electron microscope image of a sample with its electrodes. On this image, we show several oscillation patterns with various angles and mean positions, the thick arrows show the direction of maximum current. at a given position. On **f**, we show that the generated current depends on both the oscillation angle and mean position. This variability, linked to the random distribution in height, position and direction of the wrinkles over the graphite strengthens the claim that wrinkles are instrumental to current generation and makes a strong argument in favor of the direct momentum transfer as the source of the current.

Raman spectroscopy To ascertain our claim that wrinkles are folded graphene structures that increase liquid friction and thus motion-induced current by a mere geometrical effect, we perform Raman spectroscopy on one transferred graphite sample and demonstrate that wrinkles show a ratio of D-peak intensity over G-peak intensity of the same order as flatter regions and that they show the usual spectroscopic properties of graphite samples. The measurements are presented on Figure S2 **g-j**, on g, we show the AFM scan of a transferred sample. On this sample, the transfer process has torn appart a top layer of graphite which is therefore showing wrinkles on top of the underlying graphite crystal (dark region). We use this particular sample to study the structural properties of wrinkles compared to a flat crystal. On **h**, we display a typical Raman spectrum measured with a 532 nm laser. On **i**, we display the G peak intensity map, revealing the inhomogeneity of thickness in the folded regions (higher G peak means thicker region). Finally, on **d**, we show the ratio of D-peak over G-peak intensity. This shows that wrinkles and folded regions are by no means defects. This analysis strengthen our theoretical treatment of wrinkles and folded regions as graphite or graphene with an enhanced corrugation.

[1] S. Faucher, Na. Aluru, M. Bazant, D. Blankschtein, A. Brozena, J. Cumings, J. Pedro de Souza, M. Elimelech, R. Epsztein, J. Fourkas, A. Govind Rajan, H.J. Kulik, A. Levy, A. Majumdar, C. Martin, M. McEldrew, R. Prasanna Misra, A. Noy, T. Anh Pham, M. Reed, E. Schwegler, Z. Siwy, Y. Wang, and M. Strano, Critical Knowledge Gaps in Mass Transport through Single-Digit Nanopores: A Review and Perspective *Journal of Physical Chemistry C*(2019)

[2] N. Kavokine, R.R. Netz, L. Bocquet, Fluids at the nanoscale: from continuum to subcontinuum transport, *Ann. Rev. Fluid Mech.* **53** 377-410 (2021)

[3] Z. Zhang, X. Li, J. Yin; Y. Xu, W. Fei, M. Xue,Q.Wang, J.Zhou and W.Guo, *Emerging Hydrovoltaic Technology.* Nature Nanotechnology(2018)

[4] S. Gosh, A. K. Sood and N. Kumar, Carbon Nanotube flow sensors, *Science*, **299**, 1042 (2003)

[5] A. Cohen, S. Gosh, A. K. Sood and N. Kumar, Carbon nanotubes provide a charge, *Science*, **300**, 1235-1236 (2003)

[6] Y. Zhao, L. Song, K. Deng, Z. Liu, Z. Zhang, Y. Yang, C. Wang, H. Yang, A. Jin, Q. Luo, C. Gu, S. Xie and L. Sun, Individual water-filled single-walled carbon nanotubes as hydroelectric power converters, *Advanced Materials*, **20**, 1772-1776 (2008)

[7] J. Rabinowitz, C. Cohen, K. L. Shepard, An electrically actuated, carbon-nanotube-based biomimetic ion pump, *Nano Letters*, **20**, 1148-1153 (2020)

[8] P. Dhiman, F. Yavari, X. Mi, H. Gullapalli, Y. Shi, P. M. Ajayan and N. Korathar, Harvesting energy from water flow over graphene, *Nano Letters*, **11**, 3123-3127 (2011)

[9] J. Yin, Z. Zhang, X. Li, J. Zhou and W. Guo, Harvesting energy from water flow over graphene?, *Nano Letters*, **12**, 1736-1741 (2012)

[10] S. H. Lee, Y. Jung, S. Kim and C.-S. Han, Flow-induced voltage generation in non-ionic liquids over monolayer graphene, *Applied Physics Letters*, **102**, 063116 (2013)

[11] K. Kuriya, K. Ochiai, G. Kalita, M. Tanemura, A. Komiya, G. Kikugawa, T. Ohara, I. Yamashita, F. Ohuchi, M. Meyyappan, S. Samukawa, K. Washio and T. Okada, Output density quantification of electriciy generation by flowing deionized water on graphene, *Applied Physics Letters*, **117**, 123905 (2020)

[12] J. Yin, X. Li, J. Yu, Z. Zhang, J. Zhou and W. Guo, Generating electricity by moving a droplet of ionic liquid along graphene, *Nature Nanotechnology*, **9**, 378-383 (2014)

[13] J. Park, S. Song, Y. Yang, S.-H. Kwon, E. Sim and Y. S. Kim, Identification of droplet-flow-induced electric energy on electrolyte-insulator-semiconductor structure, *Journal of the American Chemical Society*, **139**, 10968-10971 (2017)

[14] J. Comtet, A. Niguès, V. Kaiser, B. Coasne, L. Bocquet and A. Siria, Nanoscale capillary freezing of ionic liquids confined between metallic interfaces and the role of electronic screening, *Nature Materials*, **16**, 634-639 (2017)

[15] A. Schlaich, D. Jin, L. Bocquet, L., B. Coasne, Electronic screening using a virtual Thomas Fermi fluid for predicting wetting and phase transitions of ionic liquids at metal surfaces, *Nature materials*, **21**, 237-245 (2022)

[16] N. Kavokine, M.-L. Bocquet and L. Bocquet, Fluctuation-induced quantum friction in nanoscale water flows, Nature, **602**, 7895 (2022)

[17] B. Coquinot, L. Bocquet, N. Kavokine, Arxiv:2205.03250 (2022).

[18] A. Fang, E. Dujardin and T. Ondarçuhu, Control of droplet size in liquid nanodispensing, *Nano Letters*, **6**, 2368-2374 (2006)

[19] L. Fabié and T. Ondarçuhu, Writing with liquid using a nanodispenser: Spreading dynamics at the sub-micron scale, *Soft Matter*, **8**, 4995-5001 (2012)

[20] https://hummink.com

[21] Castro Neto, A. H., F. Guinea, N. M. R. Peres, K. S. Novoselov, and A. K. Geim The Electronic Properties of Graphene Reviews of Modern Physics **81**, (2009)

[22] J. Pei, J. Huang, Z. Huang and K. Liu, Liquid flow-induced electricity in carbon nanomaterials, *Sustainable Energy Fuels*, **3**, 599-610 (2019)

[23] Roddaro, S., Pingue, P., Piazza, V., Pellegrini, V. and Beltram, F. The Optical Visibility of Graphene: Interference Colors of Ultrathin Graphite on SiO 2 *Nano Letters* (2007)

[24] Pizzocchero, F. et al. The hot pick-up technique for batch assembly of van der Waals heterostructures *Nature communications*, 11894 (2016)

[25] B. N. J. Persson, U. Tartaglino, E. Tosatti and H. Ueba, Electronic friction and liquid flow-induced voltage in nanotubes, *Physical Review B*, **69**, 235410 (2004)

[26] J. K. Moon, J. Jeong, D. Lee and H. K. Pak, Electrical power generation by mechanically modulating electrical double layers, *Nature communications*, **4**, 1487 (2013)

[27] Rastikian, J. et al. High performance room temperature p-type injection in few-layered tungsten diselenide films from cobalt and palladium contacts *Material Research Express* (2019).

[28] A. Gruneis, C. Attaccalite, L. Wirtz, H. Shiozawa, R. Saito, T. Pichler, A. Rubio, Tight-binding description of the quasiparticle dispersion of graphite and few-layer graphene, Physical Review B, **78**, 1–16 (2008)

[29] F. Guinea, M. I. Katsnelson, M. A. H. Vozmediano, Midgap states and charge inhomogeneities in corrugated graphene, Physical Review B, **77**, 1–8 (2008)

[30] J. C. Charlier, J. P. Michenaud, P. Lambin, Tight-binding density of electronic states of pregraphitic carbon, Physical Review B, **46**, 4540–4543 (1992)

[31] G. Gonella *et al.*, Water at charged interfaces, *Nature Rev. Chem.* **5** 466-485 (2021).

[32] P. Král and M. Shapiro, Nanotube electron drag in flowing liquids, *Physical Review Letters*, **86**, 131-134 (2014)

[33] N. Liu, Z. Pan, L. Fu, C. Zhang, B. Dai and Z. Liu, The origin of wrinkles on transferred graphene, *Nano Research*, **4**, 996 (2011)

[34] S. Deng and V. Berry, Wrinkled, rippled and crumpled graphene: An overview of formation mechanism, electronic properties and applications, *Materials Today*, **19**, 197-212 (2016)

[35] Nika, D. L. and Pokatilov, E. P. and Askerov, A. S. and Balandin, A. A., Phonon thermal conduction in graphene: Role of Umklapp and edge roughness scattering, Phys. Rev. B, **15**, 155413 (2009)

[36] P.G. Klemens and D.F. Pedraza, Thermal conductivity of graphite in the basal plane, *Carbon*, **4**, 735-741, 32 (1994)

[37] Ochoa, H. and Castro, Eduardo V. and Katsnelson, M. I. and Guinea, F. Temperature-dependent resistivity in bilayer graphene due to flexural phonons, *Phys. Rev. B*, **83**, 23 (2011)

[38] Cong, X., Li, Q.-Q., Zhang, X., Lin, M.-L., Wu, J.-B., Liu, X.-L., Venezuela, P. and Tan, P.-H. Probing the Acoustic Phonon Dispersion and Sound Velocity of Graphene by Raman Spectroscopy, *Carbon*, **149**, (2019)

[39] A. Gruneis, C. Attaccalite, L. Wirtz, H. Shiozawa, R. Saito, T. Pichler, A. Rubio, Tight-binding description of the quasiparticle dispersion of graphite and few-layer graphene, *Physical Review B*, **78**, 1–16 (2008)

[40] F. Guinea, M. I. Katsnelson, M. A. H. Vozmediano, Midgap states and charge inhomogeneities in corrugated graphene, *Physical Review B*, **77**, 1–8 (2008)

[41] J. C. Charlier, J. P. Michenaud, P. Lambin, Tight-binding density of electronic states of pregraphitic carbon, *Physical Review B*, **46**, 4540–4543 (1992)

[42] Bae, Jaehyeong, Min Soo Kim, Taegon Oh, Bong Lim Suh, Tae Gwang Yun, Seungjun Lee, Kahyun Hur, Yury Gogotsi, Chong Min Koo, and Il-Doo Kim Towards Watt-Scale Hydroelectric Energy Harvesting by $Ti_3C_2T_x$-Based Transpiration-Driven Electrokinetic Power Generators, *Energy and Environmental Science* , **15** (2022)

[43] Neumann, Reichardt, Venezuela, Drogeler, Banszerus, Schmitz, Watanabe, Taniguchi, Mauri, Beschoten, Rotkin and Stampfer Raman spectroscopy as probe of nanometre-scale strain variations in graphene, *Nature Communications*, (2015)

[44] Lynden-Bell et al, Electrode screening by ionic liquids,, *Phys. Chem. Chem. Phys* , **15** (2012)

[45] Greenwood et al, Effects of Layering and Supporting Substrate on Liquid Slip at the Single-Layer Graphene Interface, *ACS Nano*,(2022)

[46] Lynden-Bell et al, Translucency and negative temperature-dependence for the slip length of water on graphene, *arXiv* ,(2022)